Determination Method of Target Material and Coil Area Based on Average Magnetic Flux Density for Metal Object Detection of Dynamic WPT

Yuya Deguchi[1], Sakahisa Nagai[2], Toshiyuki Fujita[3], Hiroshi Fujimoto[4]
Graduate School of Frontier Science
The University of Tokyo
Kashiwa, Japan
[1]deguchi.yuya20@ae.k.u-tokyo.ac.jp, [2]nagai-saka@edu.k.u-tokyo.ac.jp, [3]t-fujita@edu.k.u-tokyo.ac.jp, [4]fujimoto@k.u-tokyo.ac.jp

***Abstract*—The detection of foreign metal objects is an essential technology to ensure the safety of the wireless power transfer (WPT) systems. The standards of required detection targets and areas have already been proposed for the static WPT (S-WPT) system. However, for the dynamic WPT (D-WPT) system, it is necessary to take into account that the magnetic field varies with the position of the receiver coil. This paper proposes a method to determine the detection targets and area for the D-WPT system. First, the average of the magnetic flux density during one charge in D-WPT is calculated using an electromagnetic field simulator. Next, the average magnetic flux density is applied to various metal plates using the S-WPT test bench, and its temperature is observed. The applying period is the same as the D-WPT driving situation. Finally, the magnetic flux density at the point when the saturation temperature of each metal reaches 80 °C is used as the threshold value, and the required detection area is determined by comparing it with the average magnetic flux density distribution. The proposal was experimentally verified using our developed WPT system, whose rated power is 20 kW. This proposal is helpful because the test can be conducted without moving the receiver coil, and can clearly define the required detection target and area for the foreign metal objects in the D-WPT system.**

***Index Terms*—eddy currents, metals, object detection, safety, foreign object detection, wireless power transfer**

I. Introduction

In recent years, wireless power transfer (WPT) technology has made remarkable progress and has been studied for numerous devices [1]–[6]. Among them, the dynamic WPT (D-WPT), which transfers power to moving electric vehicles (EVs), is attracting attention as a helpful technology for realizing a decarbonized society because it can extend their cruising range and reduce their battery weight [7]–[9].

However, safety assurance is essential for realizing this technology in society, and a problem that threatens safety is the intrusion of foreign metal objects. In the WPT systems, a foreign metal object between coils causes eddy current loss, which leads to a decrease in the system efficiency and heat generation in the metal. Especially, the generated heat damages the road equipment. For high-power WPT systems, this problem is serious and should be addressed. Therefore, there have been many discussions for foreign metal objects in a WPT system, such as detection methods, targets, and area [10]–[23].

For the detection methods, measuring the parameters' change of the WPT circuit [12], [13], adding a detection circuit placed on a transmitter coil [15]–[18], and using external devices such as cameras and sensors [19], [20] have been proposed. For the detection targets, the Society of Automotive Engineers (SAE) and the International Electrotechnical Commission (IEC) have proposed the standards for detection targets and criteria [21], [22]. For the detection area, the magnetic flux density threshold is determined as the value at which the saturation temperature of the metal reaches the SAE criterion (80 °C). The detection area is defined by the magnetic flux density distribution on the transmitter coil that exceeds the threshold [23].

However, all of the above discussions are for the static WPT (S-WPT) system, which transfers power to stationary EVs. This paper proposes a method to determine the detection target and detection area of a foreign metal object for the D-WPT system.

In the D-WPT system, multiple coils are embedded in the road, and EVs run through the road. Since each coil transfers power to EVs intermittently, each power transfer time is shorter than the S-WPT. Therefore, the amount of heat generation in the metal in the D-WPT system is different from that of S-WPT, and the detection target may also be different. In addition, the distribution of magnetic flux density on the transmitter coil changes as the receiving coil moves. Therefore, it is impossible to determine a constant threshold for magnetic flux density as the previous research on the S-WPT system [23].

We propose using the average magnetic flux density distribution for the movement of the receiver coil by electromagnetic simulation software. By applying this average magnetic flux density intermittently according to the power transfer situation in the D-WPT system, the temperature rise of a foreign metal object in the D-WPT system can be reproduced using the S-WPT system.

The proposed method applied our developed D-WPT system, whose rated power is $20\,\mathrm{kW}$. The average magnetic flux density distribution in our D-WPT system is calculated in the electromagnetic field simulator JMAG-Designer. To determine the threshold value to be compared to that distribution, constant magnetic flux density applied intermittently to the various metal plates of $50\,\mathrm{mm} \times 50\,\mathrm{mm} \times 3\,\mathrm{mm}$ using the S-WPT experimental bench. The magnetic flux density threshold is defined as the value when the temperature of the metal plates reaches $80\,^{\circ}\mathrm{C}$. By comparing the threshold of magnetic flux density with the distribution of average magnetic flux density calculated by the software, the required detection area on the transmitter coil in the D-WPT system was determined.

The result shows that the performance required for the detection methods in the D-WPT system can be tested by the S-WPT experimental bench. The contribution of this paper is that the required detection target and area of the D-WPT system can be determined from small-scale experiments of the S-WPT system and the average magnetic flux density distribution without large experimental setups.

II. FOREIGN METAL OBJECTS IN DYNAMIC WIRELESS POWER TRANSFER

A. Power losses in metal objects

The temperature of the metal rises according to the iron loss P, and it can be divided into three main components as follows [24]:

$$P = P_h + P_e + P_{ec} = afB_p^x + ef^2B_p^{1.5} + bf^2B_p^2, \tag{1}$$

where P_h is a hysteresis loss, P_e is an excess loss, and P_{ec} is an eddy current loss. B_p is a peak value of the magnetic flux density expressed as a product of the vacuum permeability μ_0, the relative permeability of the metal μ_r, and a magnetic field $H.f$ is a frequency of the magnetic flux density and x is the Steinmetz coefficient. a, e, and b are the coefficients of a hysteresis loss, an eddy current loss, and an excess loss, respectively.

P_e is negligible in (1) since e is close to 0 [24]. As for the standard materials with the same volume, the range of x is from 1.75 to 2.1, and the range of a/b is from 100 to 500 [23], [24]. Therefore, P_{ec} is much larger than P_h and P_e at high frequencies such as $85\,\mathrm{kHz}$, the standard operating frequency of D-WPT [21]. From the above, the main component of the iron loss P is eddy current loss P_{ec} in this case.

B. Heat generation of foreign metal objects in WPT system

The eddy current loss per unit volume $P_{ec_{unit}}$ can be expressed as follows [25]:

$$P_{ec_{unit}} = k_e \frac{R^2B_p^2f^2}{\rho}, \tag{2}$$

where k_e is the redefined eddy current loss coefficient, R is a radius of the eddy current path, and ρ is a resistivity of the metal. The amount of heat J produced by a metal of volume V for single power transmission is expressed as follows:

$$J = P_{ec_{unit}}Vt_{trans} = k_e \frac{R^2B_p^2f^2}{\rho}Vt_{trans}, \tag{3}$$

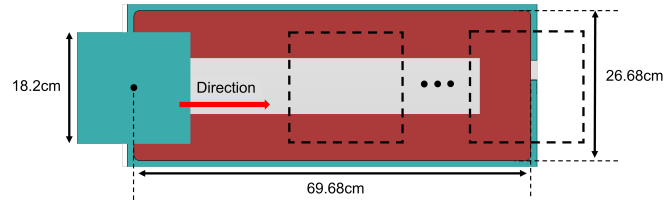

Fig. 1. Power transmitter and receiver coils used in the simulation.

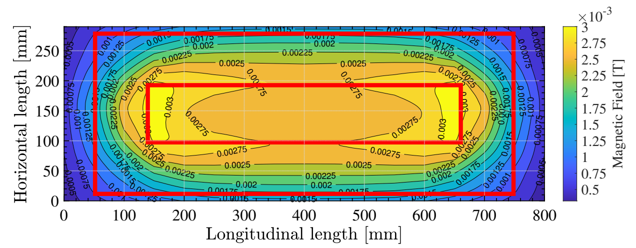

Fig. 2. 2D contour graph of $B_{p_{ave}}$ on the transmitter coil. The red rectangle indicates the area where the litz wire of the transmission coil is present.

where t_{trans} is a time of the power transfer. In the S-WPT system, t_{trans} is long enough that J eventually balances the amount of heat dissipation during power transmission, and the metal's temperature will be saturated. If both the shape and type of the foreign metal object are fixed, the saturation temperature only depends on B_p. Therefore, the threshold value of the magnetic flux density B_{th} can be determined when a certain metal object's temperature reaches the threshold. The required detection area on the transmitter coil for the metal object can be derived by comparing B_{th} with the magnetic flux density distribution [23].

However, in the D-WPT system, t_{trans} is much shorter than that of S-WPT, and the power transfer of each coil is intermittent. Therefore, the saturation temperature of the metal depends on the power transfer interval and will be lower than that of S-WPT for the same power scale. In addition, a magnetic field density distribution on a transmitter coil changes with the receiver coil's positions. For simplicity, we assume that all cars travel on the transmission coil without misalignment. In this case, B_p in (3) becomes a time function $B_p(t)$, and the amount of heat generation in the metal is expressed as the integral of $B_p(t)$ over the supplying time t_{trans} as follows:

$$J = \int_0^{t_{trans}} k_e \frac{R^2B_p^2(t)f^2}{\rho}V dt \tag{4}$$

In this case, the detection area cannot be determined by a simple comparison with a threshold value B_{th}.

C. Average magnetic flux density distribution in D-WPT

To solve this problem, we calculate the average magnetic flux density $B_{p_{ave}}$ for the movement of the receiver coil. If the power scale and the transfer interval are fixed, $B_{p_{ave}}$ depends only on the position of the receiver coil. In this paper, the magnetic flux density distribution on the transmission coil for each position of the receiving coil was calculated and averaged using electromagnetic field simulation software. Using $B_{p_{ave}}$, (4) can be transformed into the same form as (3) as follows:

$$J \simeq k_e \frac{R^2 B_{p_{ave}}^2 f^2}{\rho} V t_{trans}. \tag{5}$$

The magnetic flux density at which the saturation temperature of the metal reaches a threshold value can be examined by the experiment with the S-WPT bench. Comparing that value with the average magnetic flux density distribution, the required detection area in the D-WPT can be determined equivalently.

When considering the required detection area for a given D-WPT system, the variables are the power transfer interval and the foreign metal object. For the power transfer interval, the longer the power supply time t_{trans} and the shorter the standby time $t_{standby}$ becomes, the larger the heat generation occurs. For foreign metal objects, from (5), the larger the relative permeability and the area intersecting with B_p become, the larger the heat generation occurs. For most detection methods, the larger the metal object's area becomes, the easier it is to detect. Therefore, as the detection target, ferromagnetic material with the smallest area whose saturation temperature reaches the threshold is suitable. If the required detection area is determined for the detection target in the situation with the largest $t_{trans}/t_{standby}$ among the assumed situations, most situations can be covered.

III. Simulation of Magnetic Flux Density Distribution

We simulated and measured the magnetic flux density distribution in the D-WPT system using the simulation software JMAG-Designer. The position of the receiver coil in the power transfer process was divided into 50 parts with respect to the distance moved, and the distribution of B_p was calculated for each pattern. $B_{p_{ave}}^2$ is defined as the average of all patterns' B_p^2. The diagram in the software is shown in Fig. 1. It is assumed that a foreign metal object has entered directly the embedded transmitter coil, and the height of the measurement point was set at $4\,\mathrm{cm}$ above the transmitter coil, which is the sum of the coil case thickness of $1\,\mathrm{cm}$ and the embedded depth of $3\,\mathrm{cm}$. The lateral displacement between the two coils and the inductance changes were neglected. Assuming a $20\,\mathrm{kW}$ D-WPT system in perfect resonance, an AC current of $40\,\mathrm{A}$ continuously flowed through each coil, and a phase difference between currents is always $90\,\mathrm{deg}$.

The result of the distribution of $B_{p_{ave}}$ as a 2D contour plot is shown in Fig. 2. The strength of the magnetic flux density is highest at the inner corners of the litz wire, with a value of $3.17\,\mathrm{mT}$.

IV. Heating experiment

A. Experimental Setup

When the size and type of foreign metal objects and driving conditions are fixed, the saturation temperature of

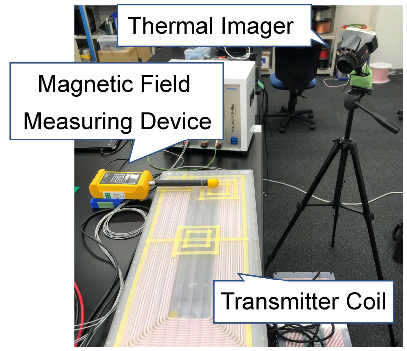

Fig. 3. Devices for the heating experiment.

Fig. 4. Metals used as foreign metal objects. Aluminum is paramagnetic. Zinc and copper are diamagnetic. Stainless, nickel and iron are ferromagnetic.

the metal is a function of the magnetic flux density from (5). A heating experiment was conducted to measure the saturation temperature by applying the magnetic flux density to six different metal plates ($50\,\mathrm{mm}\ \times\ 50\,\mathrm{mm}\ \times 3\,\mathrm{mm}$). The magnetic flux density at the metal object's position was measured using a magnetic field exposure level tester (Narda ELT-400). The current was applied using a full-bridge inverter, and the frequency is $85\,\mathrm{kHz}$. The metal plates were coated with black body spray (emissivity: 0.95), and the temperature was measured with a thermal imager (Testo 881-2). The appearance of the experiment is shown in Fig. 3. The used metal plates are shown in Fig. 4, and the parameters of the metal are shown in Table. I.

The parameters of the coils used are listed in Table.II. The driving conditions were assumed to be traffic jams, with an applied time of $504\,\mathrm{ms}$ and a standby time of $3600\,\mathrm{ms}$. Assuming that cars were constantly coming as the worst-case condition, intermittent power supply was continued until the metal temperature was saturated. Following the SAE standard, the detection targets are metals whose saturation temperature is $80\,^{\circ}\mathrm{C}$ or higher. In order to safely experiment, low voltage is applied with no receiving coil and low input impedance. In addition, if the temperature exceeded $90\,^{\circ}\mathrm{C}$ during the experiment, the experiment was terminated.

B. Required detection target and area in D-WPT

The saturation temperature of each metal when $3.0\,\mathrm{mT}$ is applied is shown in Fig. 5. $3.0\,\mathrm{mT}$ is near the value of the

TABLE I
PARAMETERS OF VARIOUS METALS (METAL TEMPERATURE IS ASSUMED TO BE 20 °C).

Magnetism	Metal	Density ρ_m [kg/m^3]	Resistivity ρ [Ω/m]	Heat capacity c	$\rho \cdot \rho_m c$	Relative permeability μ_r
Ferromagnetic	Iron	7.87 $\times 10^3$	1.00 $\times 10^{-7}$	4.61 $\times 10^2$	0.36	5.00 $\times 10^3$
	Nickel	8.90 $\times 10^3$	6.99 $\times 10^{-8}$	4.61 $\times 10^2$	0.28	6.00 $\times 10^2$
Diamagnetic	Copper	8.96 $\times 10^3$	1.68 $\times 10^{-8}$	4.19 $\times 10^2$	0.063	1
	Zinc	7.14 $\times 10^3$	6.02 $\times 10^{-8}$	3.83 $\times 10^2$	0.16	1
Paramagnetic	Aluminum	2.70 $\times 10^3$	2.65 $\times 10^{-8}$	9.00 $\times 10^2$	0.064	1
Alloy	Stainless Steel	7.90 $\times 10^3$	7.40 $\times 10^{-7}$	4.60 $\times 10^2$	2.67	> 1

TABLE II
TRANSMITTER COIL SPECIFICATIONS

Coil Length	0.697 m
Coil Width	0.267 m
Self-Inductance	200.7 µH
Resistance (w/Capacitor)	159.8 mΩ
Operating Frequency	85 kHz
Number of Turns	13

highest magnetic flux density area in Fig. 2. The saturation temperature of the diamagnetic and paramagnetic materials did not reach 80 °C, but the ferromagnetic materials all exceeded 90 °C.

In order to confirm the relationship between the permeability and the saturation temperature, a low magnetic flux density is applied to the ferromagnetic materials and measure the saturation temperature. Fig. 6 shows the saturation temperature of the ferromagnetic material when 1.23 mT is applied. The higher the relative permeability of the metal becomes, the higher the saturation temperature of the metal becomes, which is consistent with (5). Therefore, a pure iron plate was used as the detection target, and the required detection area was determined.

Fig. 7 shows a graph of the magnetic flux density and saturation temperature, approximated quadratically by the least-squares method based on (3). From the lower limit of the 95% confidence interval in Fig. 7, in the area where the average magnetic flux density is 1.21 mT or higher, the saturation temperature of the pure iron plate reaches 80 °C. In Fig. 8, the area where the average flux density exceeds this threshold is shown as a colored area.

Since other metals have lower specific permeability than pure iron, they reach 80 °C only in a limited area where the magnetic flux density is greater than this threshold. In addition, the faster vehicle speeds also increase the inter-vehicular distance, but the transmitter coil length does not change. Therefore, the faster vehicle speeds generally result in a smaller $t_{trans}/t_{standby}$ and less heat generation. From the above, the required detection area in Fig. 8 covers all areas where the foreign metal object of the same shape reaches 80 °C in situations where the vehicle speed is greater than 5 km/h. Therefore, the detection area obtained in this study is valid for other metal objects of the same shape. The detection area also can be identified for additional shapes or types of metal objects by following the same procedure.

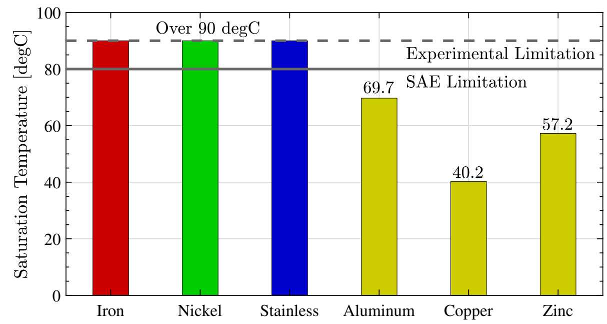

Fig. 5. The saturation temperature of each metal when 3 mT is applied.

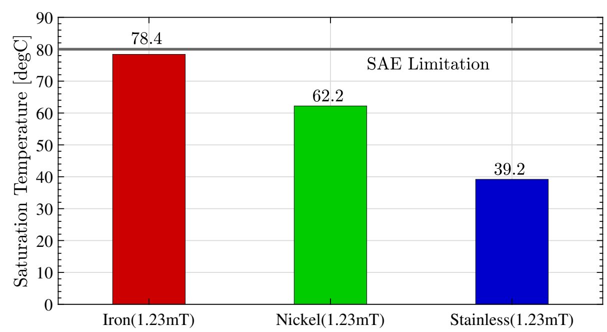

Fig. 6. The saturation temperature of ferromagnetic metal when 1.23 mT is applied.

V. CONCLUSION

This paper proposed a method to determine the detection targets and areas to be detected for the foreign metal objects in the D-WPT system. The magnetic flux density changes depending on the position of the receiving coil in the D-WPT system. Therefore, we averaged all magnetic flux density distributions for the movement of the receiver coil during a single power transfer using simulation software and made a contour plot of the average magnetic flux density. We conducted heating experiments on our S-WPT system assumed for traffic congestion (Vehicle speed: 5 km/h, Inter-vehicular distance: 5 m). By applying the magnetic flux density under the same feeding conditions as the D-WPT, the relationship between the magnetic flux density and the saturation temperature of the metal object can be obtained. As a result, it was found that only ferromagnetic materials generated heat in a metal plate with 50 mm × 50 mm ×3 mm, and that pure iron plate which has the highest saturation temperature among them must be detected in the area where more than 1.21 mT is applied as

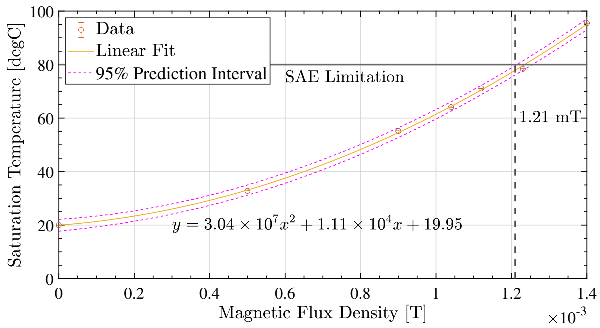

Fig. 7. Graph of magnetic flux density and saturation temperature of the iron plate.

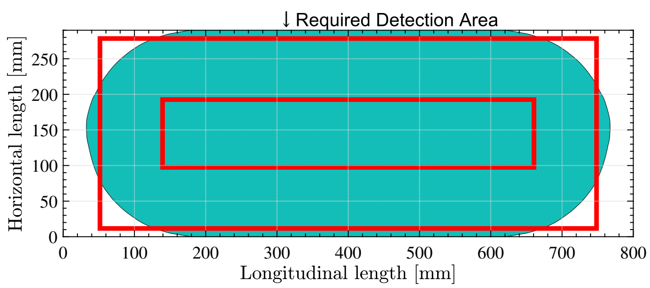

Fig. 8. The colored area indicates the required detection area for the iron plate.

an average on the transmitter coil. This method can reproduce the heat generation of metals in D-WPT by the S-WPT bench and the magnetic field analysis by simulation. It is helpful to determine required detection targets and areas for foreign metal objects in the D-WPT system and can be used to validate metal object detection methods.

Acknowledgment

This work was partly supported by JST-Mirai Program Grant Number JPMJMI21E2, JSPS KAKENHI Grant Number JP18H03768, and a project, JPNP21005, subsidized by the New Energy and Industrial Technology Development Organization (NEDO), Japan.

References

[1] D. Gunji, T. Imura, and H. Fujimoto, "Basic study of transmitting power control method without signal communication for wireless in-wheel motor via magnetic resonance coupling," in *2015 IEEE International Conference on Mechatronics (ICM)*, 2015, pp. 317–322.

[2] M. Sato, G. Yamamoto, D. Gunji, T. Imura, and H. Fujimoto, "Development of wireless in-wheel motor using magnetic resonance coupling," *IEEE Transactions on Power Electronics*, vol. 31, no. 7, pp. 5270–5278, 2016.

[3] K. Kusaka and J. ichi Itoh, "Development trends of inductive power transfer systems utilizing electromagnetic induction with focus on transmission frequency and transmission power," *IEEJ Journal of Industry Applications*, vol. 6, no. 5, pp. 328–339, 2017.

[4] T. Koyama, K. Umetani, and E. Hiraki, "Design optimization method for the load impedance to maximize the output power in dual transmitting resonator wireless power transfer system," *IEEJ Journal of Industry Applications*, vol. 7, no. 1, pp. 49–55, 2018.

[5] H. Matsumoto, T. Zaitsu, R. Noborikawa, Y. Shibako, and Y. Neba, "Control for maximizing efficiency of three-phase wireless power transfer systems at misalignments," *IEEJ Journal of Industry Applications*, vol. 9, no. 4, pp. 401–407, 2020.

[6] H. Ishida, T. Kyoden, and H. Furukawa, "Application of parity-time symmetry to low-frequency wireless power transfer system," *IEEJ Journal of Industry Applications*, vol. 11, no. 1, pp. 59–68, 2022.

[7] V.-D. Doan, H. Fujimoto, T. Koseki, T. Yasuda, H. Kishi, and T. Fujita, "Simultaneous optimization of speed profile and allocation of wireless power transfer system for autonomous driving electric vehicles," *IEEJ Journal of Industry Applications*, vol. 7, no. 2, pp. 189–201, 2018.

[8] V. Cirimele, M. Diana, F. Bellotti, R. Berta, N. E. Sayed, A. Kobeissi, P. Guglielmi, R. Ruffo, M. Khalilian, A. La Ganga, J. Colussi, and A. D. Gloria, "The fabric ict platform for managing wireless dynamic charging road lanes," *IEEE Transactions on Vehicular Technology*, vol. 69, no. 3, pp. 2501–2512, 2020.

[9] O. Shimizu, S. Nagai, T. Fujita, and H. Fujimoto, "Potential for CO2reduction by dynamic wireless power transfer for passenger vehicles in Japan," *Energies*, vol. 13, no. 13, 2020.

[10] J. Lu, G. Zhu, and C. C. Mi, "Foreign object detection in wireless power transfer systems," *IEEE Transactions on Industry Applications*, vol. 58, no. 1, pp. 1340–1354, 2022.

[11] J. Stillig, M. Edviken, and N. Parspour, "Overview and aspects of foreign object detection in wireless power transfer applications," in *2020 IEEE Wireless Power Transfer Conference (WPTC)*, 2020, pp. 380–383.

[12] S. Fukuda, H. Nakano, Y. Murayama, T. Murakami, O. Kozakai, and K. Fujimaki, "A novel metal detector using the quality factor of the secondary coil for wireless power transfer systems," *2012 IEEE MTT-S International Microwave Workshop Series on Innovative Wireless Power Transmission: Technologies, Systems, and Applications, IMWS-IWPT 2012 - Proceedings*, no. mm, pp. 241–244, 2012.

[13] H. Jafari, M. Moghaddami, and A. I. Sarwat, "Foreign Object Detection in Inductive Charging Systems Based on Primary Side Measurements," *IEEE Transactions on Industry Applications*, vol. 55, no. 6, pp. 6466–6475, 2019.

[14] M. Ote, S. Jeong, and M. M. Tentzeris, "Foreign object detection for wireless power transfer based on machine learning," in *2020 IEEE Wireless Power Transfer Conference (WPTC)*, 2020, pp. 476–479.

[15] H. Zhang, D. Ma, X. Lai, X. Yang, and H. Tang, "The Optimization of Auxiliary Detection Coil for Metal Object Detection in Wireless Power Transfer," *2018 IEEE PELS Workshop on Emerging Technologies: Wireless Power Transfer, Wow 2018*, pp. 1–6, 2018.

[16] V. X. Thai, G. C. Jang, S. Y. Jeong, J. H. Park, Y. S. Kim, and C. T. Rim, "Symmetric Sensing Coil Design for the Blind-Zone Free Metal Object Detection of a Stationary Wireless Electric Vehicles Charger," *IEEE Transactions on Power Electronics*, vol. 35, no. 4, pp. 3466–3477, 2020.

[17] S. Y. Chu, X. Zan, and A.-T. Avestruz, "Electromagnetic model-based foreign object detection for wireless power transfer," *IEEE Transactions on Power Electronics*, vol. 37, no. 1, pp. 100–113, 2022.

[18] S. Son, S. Lee, J. Rhee, Y. Shin, S. Woo, S. Huh, C. Lee, and S. Ahn, "Foreign object detection of wireless power transfer system using sensor coil," in *2021 IEEE Wireless Power Transfer Conference (WPTC)*, 2021, pp. 1–4.

[19] J. W. Jeong, S. H. Ryu, B. K. Lee, and H. J. Kim, "Tech tree study on foreign object detection technology in wireless charging system for electric vehicles," *INTELEC, International Telecommunications Energy Conference (Proceedings)*, vol. 2016-Septe, pp. 1–4, 2016.

[20] X. Liu, C. Liu, W. Han, and P. W. Pong, "Design and Implementation of a Multi-Purpose TMR Sensor Matrix for Wireless Electric Vehicle Charging," *IEEE Sensors Journal*, vol. 19, no. 5, pp. 1683–1692, 2019.

[21] *Society of Automotive Engineers recommended practice J2954: Wireless Power Transfer for Light-Duty Plug-In/Electric Vehicles and Alignment Methodology*. Society of Automotive Engineers International, 2020.

[22] *IEC TS 61980-3: Electric vehicle wireless power transfer (WPT) systems – Part 3: Specific requirements for the magnetic field wireless power transfer systems*. International Electrotechnical Commission, 2019.

[23] Y. Sun, G. Wei, K. Song, X. Huang, Q. Zhang, and C. Zhu, "Determination foreign object detection area in electric vehicle wireless charging system based on thermal temperature rise characteristic," *2020 IEEE Transportation Electrification Conference and Expo, ITEC 2020*, pp. 258–261, 2020.

[24] A. Boglietti, A. Cavagnino, M. Lazzari, and M. Pastorelli, "Predicting iron losses in soft magnetic materials with arbitrary voltage supply: an

engineering approach," *IEEE Transactions on Magnetics*, vol. 39, no. 2, pp. 981–989, 2003.

[25] T. Imura, *Wireless Power Transfer: Using Magnetic and Electric Resonance Coupling Techniques*. Springer Nature Singapore Ltd., 2020.